59825 88462

Revised Manuscript.docx

Assignment

Class

University

Document Details

Submission ID

trn:oid:::1:2997978967

Submission Date

Sep 4, 2024, 2:02 PM UTC

Download Date

Sep 4, 2024, 2:03 PM UTC

File Name

Revised_Manuscript.docx

File Size

1.5 MB

19 Pages

4,842 Words

29,624 Characters

*% detected as AI

AI detection includes the possibility of false positives. Although some text in this submission is likely AI generated, scores below the 20% threshold are not surfaced because they have a higher likelihood of false positives.

Caution: Review required.

It is essential to understand the limitations of AI detection before making decisions about a student's work. We encourage you to learn more about Turnitin's AI detection capabilities before using the tool.

Frequently Asked Questions

How should I interpret Turnitin's AI writing percentage and false positives?

The percentage shown in the AI writing report is the amount of qualifying text within the submission that Turnitin's AI writing detection model determines was either likely AI-generated text from a large-language model or likely AI-generated text that was likely revised using an AI-paraphrase tool or word spinner.

False positives (incorrectly flagging human-written text as AI-generated) are a possibility in AI models.

AI detection scores under 20%, which we do not surface in new reports, have a higher likelihood of false positives. To reduce the likelihood of misinterpretation, no score or highlights are attributed and are indicated with an asterisk in the report (*%).

The AI writing percentage should not be the sole basis to determine whether misconduct has occurred. The reviewer/instructor should use the percentage as a means to start a formative conversation with their student and/or use it to examine the submitted assignment in accordance with their school's policies.

What does 'qualifying text' mean?

Our model only processes qualifying text in the form of long-form writing. Long-form writing means individual sentences contained in paragraphs that make up a longer piece of written work, such as an essay, a dissertation, or an article, etc. Qualifying text that has been determined to be likely AI-generated will be highlighted in cyan in the submission, and likely AI-generated and then likely AI-paraphrased will be highlighted purple.

Non-qualifying text, such as bullet points, annotated bibliographies, etc., will not be processed and can create disparity between the submission highlights and the percentage shown.

Prediction of phases and mechanical properties of magnesium-based high-entropy alloys using machine learning

Abstract

Objectives: To predict phases and mechanical properties of Mg-Al-Cu-Mn-Zn alloys and to validate the results.

Methods: In this study, 29 predictor features of the alloys were examined based on dataset drawn from relevant publications. The correlation of selected predictor features with mechanical properties of Mg-Al-Cu-Mn-Zn alloy were evaluated. New features specific to vehicle and aerospace applications. Feature selection schemes involving four machine learning (ML) classifiers that included artificial neural networks (ANN), linear discriminant analysis (LDA), random forest regression (RF) and k-nearest neighbours (k-NN) were adopted. Tensile test was carried out based on ASTM E8 standard.

Results: Results of correlation of features showed that specific strengths and specific modulus of the alloys were strongly and positively correlated with composition of alloying elements but strongly and negatively correlated with composition of magnesium. The results also revealed that homogenization temperatures and time were weakly correlated with the mechanical properties and phases while electronegativity difference and VEC had significant positive correlation. ANN was the best performing classifier followed by k-NN, LDA, and lastly RF with prediction accuracy on test data of 98.7%, 98.1%, 97.9% and 97.8%, respectively. The validity and applicability of the model was tested with three magnesium-based alloys: Mg-80-Al-10-Cu-5-Mn-5-Zn-0, Mg-80-Al-5-Cu-5-Mn-5-Zn-5 and Mg-91.2-Al-8.3-Cu-0-Mn-0.15-Zn-0.35 and compared with findings in literature. The model had higher prediction accuracies compared to previous ML models used on magnesium alloys. The model was then used to predict phases in the Mg-89.43-Al-8.16-Cu-0.34-Mn-0.25-Zn-1.81 alloy and it accurately predicted presence of $Mg_{17}Al_{12}$, Mg_2Si, MgZn and $MgZn_2$. Results of simulation in MatCalc version 6.04 also verified presence of the phases. The phases were further confirmed through SEM/EDS analysis.

Conclusions: Dominant strengthening phases were $Mg_{17}Al_{12}$, Mg_2Si, MgZn and $MgZn_2$. Predicted yield strength, ultimate tensile strength and Young's modulus were within the range of experimental results.

Keywords: Magnesium alloys; Phase prediction; Machine learning; Predictor features; Mechanical properties

1. Introduction

A new area of interest in material science is modelling and development of materials with enhanced mechanical properties (Stergiou et al., 2023). One such interest is to be able to predict mechanical properties from compositions and phases of modern light alloys with low densities and high strength-to-weight ratios applicable in aerospace and light-vehicle industries (Feng et al., 2016). The light metals include high entropy alloys (HEAs) of aluminium, magnesium, titanium, and beryllium (Behera et al., 2022; Feng et al., 2016). Traditional methods for developing materials, such as empirical trial and error, may be replaced by machine learning (ML) techniques and artificial intelligence that are capable of predicting alloy phases and mechanical properties (Feng et al., 2016). Research has shown that mechanical properties of HEAs can be improved through understanding of phases present in the alloy materials. Over the years, ML has been applied to various tasks of phase and mechanical property predictions that are computationally intensive with good results (Machaka, 2021).

ML algorithms provide fast and low-cost approach compared to traditional techniques of material design, phase prediction, analysis and modelling (Ford et al., 2021; Machaka, 2021). There is great research focus on prediction of phases and mechanical properties of high-entropy alloys of light metals (Qiao et al., 2021; Xiong et al., 2023). Exploration of phases and mechanical properties of magnesium alloys has risen over the years to because of lowest density of magnesium among other light metals and opportunity to reduce dead weight of vehicles, aircraft and spacecraft (Reza Kashyzadeh et al., 2023). There is a rising interest in Mg-Al-Cu-Mn-Zn that has seen improved mechanical properties based on varied percentages of the alloying elements and strengthening phases (Tun et al., 2019). However, existing ML-based research on high-entropy alloys lacks standardization, focuses generally, and fail to address the promising Mg-Al-Cu-Mn-Zn for lightweight, high-strength applications.

Previous research identified phases that were commonly associated with magnesium alloys. The phases included: $Mg_{17}Al_{12}$ in their gamma and beta states (Yamanoglu et al., 2021), laves phases such as Mg_2Cu and $MgCu_2$ (Fan et al., 2021), and $MgZn_2$ and Mg_2Zn_{11} (Bilbao et al., 2022). Other phases identified in literature and put in CALPHAD databases included β_Al_3Mg_2, θ_Al_2Cu, Al_2Cu_3_D, Al_9Cu_{11}_Z,AlCu_ζ, AlCu_G_D83, AlCuMg_V (Tayyebi et al., 2021). Previous research such as Pei et al. (2020), Li and Tsai (2020), Li and Guo (2019) focused on crystal structures associated with alloy phases rather than actual phases.

Recent research efforts to predict phases and mechanical properties of magnesium alloys focused on understanding their phase transformations and mechanical properties under various conditions (Chen et al., 2020, 2019a, 2019b). Chen et al. (2019a) studied constitutive behaviour of AZ80 magnesium alloy during hot deformation using a segmented model that outperformed Arrhenius and Johnson–Cook models. The research provided a comprehensive understanding of high-temperature deformation characteristics relating to alloy phases. Chen et al. (2019b) explored the effects of ultrasonic vibration on the casting process of AZ80 alloy and found significant differences in mechanical properties in relation to phase. Chen et al. (2020) showed that Mg-Zn-Y alloy subjected to dual-frequency ultrasonic field result in improved mechanical strength, and corrosion resistance as a result of quasi-crystals. These studies collectively advance the prediction and optimization of phases and mechanical properties in magnesium alloys. These studies did not focus on specific strength and specific modulus and did not focus Mg-Al-Cu-Mn-Zn alloys. They also did not use ML algorithms.

Various researchers focused specifically on strength and phases of magnesium alloys using ML prediction techniques. Liu et al. (2021) developed high-strength Mg cast alloys by iteratively optimizing the composition and heat treatment condition based on a surrogate model that evolved with new data. Pei et al. (2020) used a random forest algorithm to investigate the deformation mechanisms and ductility of Mg. However, the specific strength and modulus was not tested in both cases. Mandal et al. (2022) used ML algorithms to predict phases in high entropy alloys and found that decision tree and SVM had 93.84% accuracy for phase prediction, and 84.32% for crystal structure classification, respectively. Most recent study by Dong et al. (2024) predicted ultimate tensile strength (UTS), yield strength (YS), elongation (EL), and hardness (HV) using Shapley additive explanations (SHAP) model and obtained accuracies of up to 93%. The study did not focus on specific strength and stiffness of the alloys for application in light vehicle and aerospace industries. It was also not specific to high entropy Mg-Al-Cu-Mn-Zn alloys.

Though ML has been used to predict phases and strengths of magnesium alloys, it has not been applied to Mg-Al-Cu-Mn-Zn alloys. Research has not focused on predicting phases, specific strength, and modulus of these alloys, despite their potential. There is need to explore these properties using ML to understand the composition-phase-strength/modulus relationship, as no single study has addressed this comprehensively. In this paper, strategies employed in previous studies on ML-based strength and phase prediction were reviewed. The objectives of the research were to predict phases, specific strengths and specific modulus of Mg-Al-Cu-

Mn-Zn alloys based on their compositions and heat treatments. A dataset of Mg-Al-Cu-Mn-Zn alloys with strength and metallurgy-specific features presented. Analysis was conducted based on a framework developed by Machaka (2021) and incorporated new features such as yield strength (YS), ultimate tensile strength (UTS), modulus of elasticity (E), specific strength at yield (spec_strength_YS), specific strength with ultimate tensile strength (spec_strength_UTS) and specific modulus (spec_mod).

2. Materials and Methods

2.1. Classification framework

Framework for analysis used in this research was based on Figure 1. Computational framework was anchored on four platforms as suggested by (Machaka, 2021). Data collection, filtering, and wrangling yielded four crystal structures, 20 phases, and 29 features. Data was processed, segmented, and split into 75% training and 25% testing. Feature selection and validation followed, with model performance tested.

2.2. Collection and selection of data

Data from research on magnesium alloys (Al, Cu, Mn, Zn) was cleaned, checked for missing data, encoded, and transformed for machine learning. Feature selection used backward elimination, forward selection, and regularization to identify significant features. New features such as density (Density_calc), change of entropy of mixing (dSmix), atomic size difference (Atom_Size_Diff), electronegativity difference (Elect_Diff) and valence electron concentration (VEC) were created using feature engineering (Bhandari et al., 2020; Machaka, 2021). dSmix was calculated based on Equation 1.

$$dSmix = -R \sum_{i=1}^{n} x_i \ln x_i \quad (1)$$

Change in enthalpy of mix was calculated using Equation 2.

$$dHmix = 4 \times \sum_{i=1, i \neq j}^{n} dH_{ij}^{mix} \, x_i \, x_j \quad (2)$$

Atomic size difference was calculated using Equation 3

$$Atom\_Size\_Diff = 100 \times \sqrt{\sum_{i=1}^{n} c_i \left(1 - \frac{r_i}{\bar{r}}\right)} \quad (3)$$

Average atomic radius was given by Equation 4.

$$\bar{r} = \sum_{i=1}^{n} x_i r_i \quad (4)$$

Valence electron concentration (VEC) was calculated based on Equation 5.

$$VEC = \sum_{i=1}^{n} C_i (VEC)_i \quad (5)$$

Electronegativity difference, χ, was calculated based on Equation 6.

$$\chi = \sum_{i=1}^{n} C_i . (\chi_i - \bar{\chi})^2 \quad (6)$$

Where, in Equations 1 – 4

R= Ideal gas constant;

x_i and x_j= Atomic percentages of the i^{th} and j^{th} elements, respectively;

r_i= Radius of the i^{th} element;

$\bar{r}$ = Average atomic radius;

χ_i= Pauling electronegativity of the ith component;

$\bar{\chi}$= Mean electronegativity for alloy system;

C_i= atomic percentage; and

$(VEC)_i$= Valence electron concentration of the i^{th} element

Iterative testing evaluated the impact of engineered features on model performance, leading to optimized results. The final data had 60 observations and 29 variables. Multicollinearity tests showed that no Variance

Inflation Factor (VIF) values exceeded 5 (see Table 1). There was moderate correlation for Atom_Size_Diff and Elect_Diff. VEC had low multicollinearity (VIF=1.27). There was no multicollinearity between the features that could affect the reliability of the predictive models as no VIF value exceeded the threshold of 5. This implied that each predictor variable, such as Atom_Size_Diff and Elect_Diff, provided unique and valuable information for the prediction without being overshadowed by correlations with other variables. The low VIF of 1.27 indicated that VEC was a stable predictor.

Though the current dataset was small, it had more features compared to other datasets of magnesium-based alloys used in machine learning (He et al., 2023; Mi et al., 2022). The research used 29 features, including alloy compositions and design parameters, to improve ML model predictions despite a small dataset (Chen et al., 2021). Feature engineering technique proposed by Machaka (2021) was used to refactor the original dataset in order to fit the learning algorithm.

2.3. Feature selection and reduction of dimensions

This study used five stages of experiments as shown in Figure 2. The first stage used all 29 features of the dataset as the baseline feature set. The second stage created four smaller feature sets by applying Boruta algorithm with the RF algorithm (Machaka, 2021). It also used recursive feature elimination based on RF regression [31]. The third stage ordered the features by declined importance applying majority-vote ranking technique for better outcomes. The fourth stage grouped the ordered-features into seven sets with the top 5, 7, 10, 13, 15, 20, 25 feature sub-sets as proposed by (Machaka, 2021). The fifth stage involved determining and validating performance of different classifiers.

2.4. ML Classifiers and performance evaluation criteria

In literature, several ML classifiers have been used in prediction of alloy phases and mechanical properties but only a few are applicable in small datasets which are associated with model over fitting or under fitting as well as and too high or too low feature dimensions (Xu et al., 2023). Algorithms for small datasets such as support vector machine (SVM), Gaussian process regression (GPR), gradient boosting decision tree (GBDT) and XGBoost though robust, have problems of inherent complexity, potential overfitting, and computational intensity. They falter with high dimensions and complex alloy data interactions. Conversely, RF, LDA, and kNN

are more apt, with RF excelling in modelling non-linearities and preventing overfitting (Xu et al., 2023). LDA maximizes class separability in limited data and helps in dimensionality reduction (see Table 3). ANN was used to model non-linear relationships and transfer learning helped to leverage it to improve performance with the small dataset. k-NN was used to classify features based on similarity measures and its problems of dimensionality was addressed using principal component analysis (PCA). RF struggles with high-dimensional data, but feature selection can mitigate this. LDA may oversimplify, yet regularization can enhance robustness. Models were trained to identify high discriminant power features. A function was defined to calculate accuracy and kappa index using a confusion matrix. Classifier performance was evaluated with three magnesium-based alloys: Mg-80-Al-10-Cu-5-Mn-5-Zn-0, Mg-80-Al-5-Cu-5-Mn-5-Zn-5, and Mg-91.2-Al-8.3-Cu-0-Mn-0.15-Zn-0.35.

2.5. Simulation in MatCalc Software

Optimal values of density, yield strength, ultimate tensile strength and stiffness were obtained from the values of percentages generated from the objective functions. MatCalc 6.04 used classical nucleation theory to estimate alloy precipitates' development and granularity, based on the Svoboda–Fischer–Fratzl–Kozeschnik (SFFK) model. Alloy composition (Mg, Al, Cu, Mn, Zn) was optimized using genetic algorithms and GRG programming in Matlab R2023b for optimal properties.

Density of Mg is given by $\rho_{Mg} = 1.738$ g/cm^3, of Al is $\rho_{Al} = 2.7$ g/cm^3, Cu is $\rho_{Cu} = 8.96$ g/cm^3, Mn is $\rho_{Mn} = 7.26$ g/cm^3 and Zn is $\rho_{Zn} = 7.133$ g/cm^3. Masses of the components were m_{Mg}, m_{Al}, m_{Cu}, m_{Mn} and m_{Zn} for magnesium, aluminium, copper, manganese and zinc. Density estimation was done using alloy formula in Equation 5 and 6 based on density of components.

$$\rho_{alloy} = \frac{m}{v} \tag{5}$$

Where,

m=mass of alloy in grams;

v=volume of alloy, cm^3,

$$m = m_{Mg} + m_{Al} + m_{Cu} + m_{Mn} + m_{Zn} \tag{6}$$

But v is the sum of volumes of the components of the alloy. Meaning volume of magnesium, $v_{Mg} = \frac{m_{Mg}}{\rho_{Mg}}$, aluminium, $v_{Al} = \frac{m_{Al}}{\rho_{Al}}$, copper, $v_{Cu} = \frac{m_{Cu}}{\rho_{Cu}}$, manganese, $v_{Mn} = \frac{m_{Mn}}{\rho_{Mn}}$ and $v_{Zn} = \frac{m_{Zn}}{\rho_{Zn}}$.

$$\rho_{alloy} = \frac{m}{v_{Mg} + v_{Al} + v_{Cu} + v_{Mn} + v_{Zn}}$$

$$= \frac{m}{\left(\frac{m_{Mg}}{\rho_{Mg}} + \frac{m_{Al}}{\rho_{Al}} + \frac{m_{Cu}}{\rho_{Cu}} + \frac{m_{Mn}}{\rho_{Mn}} + \frac{m_{Zn}}{\rho_{Zn}}\right)} \quad (7)$$

Percentages of the components by weight were $p_{Mg} = \frac{m_{Mg}}{m} * 100\%$, $p_{Al} = \frac{m_{Al}}{m} * 100\%$, $p_{Cu} = \frac{m_{Cu}}{m} * 100\%$, $p_{Mn} = \frac{m_{Mn}}{m} * 100\%$, and $p_{Zn} = \frac{m_{Zn}}{m} * 100\%$ for magnesium, aluminium, copper, manganese and zinc

$$\rho_{alloy} = \frac{100}{\frac{p_{Mg}}{\rho_{Mg}} + \frac{p_{Al}}{\rho_{Al}} + \frac{p_{Cu}}{\rho_{Cu}} + \frac{p_{Mn}}{\rho_{Mn}} + \frac{p_{Zn}}{\rho_{Zn}}} \quad (8)$$

The specific strength at yield, $\frac{YS}{\rho_{alloy}}$, $\frac{UTS}{\rho_{alloy}}$ and specific modulus $\frac{E}{\rho_{alloy}}$became the objective functions for genetic algorithm implementation of multi-objective. The aim was to maximize each as shown in Equation 9.

$$Maximize \begin{cases} \frac{YS}{\rho_{alloy}} = \frac{k_1}{(k_2)^{\frac{tau_1}{tau_2}}} \left(\rho_{alloy}\right)^{\left(\frac{tau_2}{tau_1}-1\right)} \\ \frac{UTS}{\rho_{alloy}} = \frac{k_3}{k_2^{\frac{tau_3}{tau_2}}} * \left(\rho_{alloy}\right)^{\left(\frac{tau_3}{tau_2}-1\right)} \\ \frac{E}{\rho_{alloy}} = \left(\frac{1}{k_2}\right)^{\frac{1}{tau_2}} * \left(\rho_{alloy}\right)^{\left(\frac{1}{tau_2}-1\right)} \end{cases} \quad (9)$$

Substituting for percentage components from Equation 8 into Equation 9, the objective functions were as shown in Equation 10.

$$Maximize\begin{cases}\dfrac{YS}{\rho_{alloy}} = \dfrac{k_1}{(k_2)^{\frac{tau_1}{tau_2}}}\left(\dfrac{100}{\frac{p_{Mg}}{\rho_{Mg}}+\frac{p_{Al}}{\rho_{Al}}+\frac{p_{Cu}}{\rho_{Cu}}+\frac{p_{Mn}}{\rho_{Mn}}+\frac{p_{Zn}}{\rho_{Zn}}}\right)^{\left(\frac{tau_2}{tau_1}-1\right)} \\ \dfrac{UTS}{\rho_{alloy}} = \dfrac{k_3}{k_2^{\frac{tau_3}{tau_2}}} * \left(\dfrac{100}{\frac{p_{Mg}}{\rho_{Mg}}+\frac{p_{Al}}{\rho_{Al}}+\frac{p_{Cu}}{\rho_{Cu}}+\frac{p_{Mn}}{\rho_{Mn}}+\frac{p_{Zn}}{\rho_{Zn}}}\right)^{\left(\frac{tau_3}{tau_2}-1\right)} \\ \dfrac{E}{\rho_{alloy}} = \left(\dfrac{1}{k_2}\right)^{\frac{1}{tau_2}} * \left(\dfrac{100}{\frac{p_{Mg}}{\rho_{Mg}}+\frac{p_{Al}}{\rho_{Al}}+\frac{p_{Cu}}{\rho_{Cu}}+\frac{p_{Mn}}{\rho_{Mn}}+\frac{p_{Zn}}{\rho_{Zn}}}\right)^{\left(\frac{1}{tau_2}-1\right)}\end{cases} \quad (10)$$

Additional parameters were essential for the kinetic simulations of precipitation, which included microstructural details and nucleation configurations. The kinetic simulation parameters encompassed thermal treatments, specifying formation at 1300°C and normalization at 400°C for one hour, alongside grain size and dislocation density considerations.

MatCalc 6.04 was used to capture precipitation domains for Mg, Al, Cu, Mn, and Zn solutes with specific trapping enthalpies. It identified precipitates like MgZn, Mg_2Cu, and MnAl phases. The thermal protocols were set to begin with casting at 1300°C, then cooling to 400°C at -0.75°C/s. Homogenization was at 400°C to reduce grain sizes, followed by quenching to 25°C at -100°C/s aimed at enhancing strength and stabilize properties.

2.6. Mechanical Tests

Mg-89.43-Al-8.16-Cu-0.34-Mn-0.25-Zn-1.81 alloy obtained from optimization results was produced using stir casting technique from source material AZ91D to which quantities of pure copper, zinc and manganese powders were added. The alloy was prepared in inert argon gas atmosphere with melt heated to 1300^0C for about 20 minutes. Pouring was done in graphite coated pre-heated steel mould. The melt was left to homogenize at 400^0C for one hour after which quenching was done in oil. The casting products were age-hardened for seven days, machined into six test samples, and prepared for tensile tests per ASTM E8. Tests in a Universal Testing Machine determined yield strength, ultimate tensile strength, and Young's Modulus, compared to predicted values.

2.7. Scanning Electron Microscopy and EDS analysis

The microstructure of the Mg-89.43-Al=8.16-Cu-0.34-Mn-0.25-Zn-1.81 alloy was characterized using scanning electron microscope (SEM) (Tun et al., 2019). Sample preparation involved polishing, embedding, mounting, dehydration, and cleaning. Samples were made electrically conductive for SEM analysis. Images formed from backscattered and secondary electrons. 50mm diameter, 4mm thick samples were prepared using nitric acid and ethanol, adhered to stubs with carbon tape, and vacuum-dried for 30 minutes.

3. Results and Discussions

3.1. Results of ML Prediction

The results revealed that homogenization temperatures and time were weakly correlated with the mechanical properties and phases while electronegativity difference and VEC had significant positive correlation. Linear discriminant analysis (LDA) results in Table 2 showed that synthesis methods significantly affected alloy properties. The properties affected included yield strength, UTS, elastic modulus (E), VEC, atomic size difference (Atom_Size_Diff), and enthalpy of mixing (dHmix). Die casting (DC) had the highest probability (0.78889), followed by solution treatment (ST_4) and solution treatment with age-hardening (ST_6) at 0.66667. Induction melting (IM) and disintegrated melt deposition (DMD) had probabilities of 0.75556 and 0.82222, respectively. Yield strength had negative coefficients in all discriminant functions, aiding class differentiation. LD1, LD2, LD3, and LD4 maximized separation between different phases or compositions. Each LD represented a direction in feature space along which the data was projected to achieve maximum separation. LD1 showed the direction that maximized the separation between the most distinct classes, often capturing the most variance. LD2 was orthogonal to LD1 and would maximize separation not captured by LD1. This process continued with each subsequent LD (LD3, LD4, LD5) being orthogonal to the previous ones and capturing the maximum separation possible.

UTS correlated positively with LD2 and LD3. Young's modulus showed mixed effects on LD1 and LD2. VEC significantly affected LD1 and LD3 but not LD2. Atom_Size_Diff greatly influenced LD1, less so LD3 and LD4 (see Table 3). dHmix had minimal impact on class differentiation. LDA results showed phase distinctions. Atomic size differences were omitted due to minor variations. Negative VEC coefficients in LD1

and LD2 highlighted its influence, while positive impact was noted in LD1. LD1 accounted for most variance of 42.97%, marking its significance in phase identification, unlike the minimal 3.71% in LD5. VEC was crucial, whereas mechanical properties had major effects on phase separation. High dHmix in magnesium alloys indicated a tendency to form distinct phases. The probability of classifying beta-$Mg_{17}Al_{12}$ in group 5 was 75.6% and in Group 4 was 82.2%. Gamma-Mg_2Si and Mg_2Cu each had the highest probability of 40% of being classified in Group 1. Similar results were found with magnesium alloys that were studied by Machaka (2021) and Tun et al. (2019).

Random forest regression yielded near-perfect categorization with negligible OOB error, predicting alloy synthesis pathways. ANN with a 6-10-5 model structure effectively predicted synthesis techniques, avoiding overfitting. Results in Figure 3 showed that ANN outperformed other models with prediction accuracy of 98.70%, precision of 98.41%, recall of 98.12%, and an F1-score of 98.70% with the proposed framework. k-NN algorithm followed closely, with slightly lower metrics across the board. The resuls that ANN had highest accuracy corroborate findings of Machaka (2021). LDA showed exceptional precision at 99.55% but lagged slightly in other areas. RF algorithm demonstrated consistent performance, though it had the lowest metrics among the evaluated algorithms. Therefore, ANN algorithm demonstrated the most balanced performance, suggesting its suitability.

3.2. Results of MatCalc Simulation

Simulation results in MatCalc 6.04 showed a high number of fine precipitates with a uniform distribution suggested consistent mechanical properties. Gamma-$Mg_{17}Al_{12}$ had an extremely low mean phase fraction and low precipitate number, implying it was residual or undeveloped. The Q-AlCuMg phase (Q_ALCUMG_P0) had a higher mean phase fraction, indicating significant presence. Other phases included Mg_2Si, MgZn, and $MgZn_2$. Thes results confirm findings of Bilbao et al. (2022) and Tayyebi et al. (2021) on intermetallic phases.

3.3. Results of SEM/EDS Analysis

At magnifications of X500 and X10,000, the microstructure in Figures 4 exposed the intricate details of the grain boundary nucleation. It showcased the presence of $Mg_{17}Al_{12}$, alpha_Mg, and Q_AlCuMg clusters. The white regions denoted the $Mg_{17}Al_{12}$ phase. The grey regions represented the alpha-Mg matrix and the dark grey

areas correspond to the Q_AlCuMg intermetallic clusters. The clarity in grain boundary nucleation of the same phases in Figures 3 and 4 suggested a repeatable and reliable microstructural pattern.

Spectrum 1 and EDS in Figure 4 showed that magnesium was predominant, with traces of oxygen. Figure 5 confirmed no peaks were omitted, representing all elements present. The EDS analysis in Figure 6 showed magnesium as the main element in Spectrum 3, with 70.96% weight and 72.91% atomic percentage. Aluminium was 20.11% by weight and 18.62% atomic percentage. The MgZn phase (6.37wt%) indicated strengthening. Presence of 10.83wt% MgO was due to surface oxidation, serving as a protective barrier against further corrosion.

3.3. Results of Tensile Test

The predicted and experimental values for the mechanical properties of the alloy closely matched, with slight variances in yield strength and Young's Modulus. The UTS showed a broader experimental range, with significant deviations at the lower end. Specific strength and modulus had more discrepancies, likely due to alloy composition, microstructure, or testing conditions. Six samples were tested, all fracturing in the middle, indicating material consistency. The load at yield was 16.17kN, with extensions at yield and fracture being 0.102439mm and 1.03mm, respectively, indicating low ductility. The predictions were reliable but could be refined for better accuracy.

4. Conclusions

The ANN framework outperformed traditional predictors due to clean, well-labelled, and unbiased data. Despite a small dataset, carefully chosen features led to good performance. SEM/EDS results showed that the tested alloy was precipitation hardened with key hardening phases being $Mg_{17}Al_{12}$, traces of Mg_2Si, MgZn, $MgZn_2$, $MgCu_2$ and the hexagonal crystal structured intermetallic alloy strengthening Q-AlCuMg phase. Presence of $Mg_{17}Al_{12}$ and Mg_2Si was correctly predicted through machine learning and simulation techniques. $Mg_{17}Al_{12}$, MgZn, $MgZn_2$ and $MgCu_2$ were correctly predicted through thermodynamic and diffusion simulation. The intermetallic LAVES_C15_P0 clusters and $Mg_{17}Al_{12}$ in the microstructure were the possible reason for low ductility of the material.

The tested material had yield strength, UTS and Young's Modulus that were close to the predicted values. Predicted yield strength was 260.2MPa while experimental values were in the range of 258-266MPa. Predicted Young's Modulus was 146GPa while experimental values fell in the range of 125.16-147.26MPa. Experimental UTS was in the range of 432.8-512.96GPa slightly below the predicted 515.96GPa. High specific strength and modulus were associated with strengthening phases of gamma- $Mg_{17}Al_{12}$, MgZn, $MgZn_2$ and $MgCu_2$.

Acknowledgment

This is to acknowledge Semi-Conductor Technologies Limited for their help with SEM/EDS scanning and analysis. This is to thank Prof Geoffrey of Penn State University for his insights and advice on phase analysis, prediction and data analysis with small datasets.

Declaration of Competing Interest

The authors do not have any competing interest to declare.

Funding

This research did not receive any specific grant from funding agencies in the public, commercial, or not-for-profit sectors.

Data Availability Statement

Data will be availed upon request.

Figures and Tables Legend

Table	Caption
Table 1	Results of test for multicollinearity
Table 2	Group means and probabilities for LDA
Table 3	LDA analysis of properties with respect to synthesis route and phases

Figure	Caption
Figure 1	Phase and mechanical properties classification framework for ML

Figures and Tables

Table 1

Results of test for multicollinearity

Density_calc	dHmix	dSmix	dGmix	Atom_Size_Diff	Elect_Diff	VEC
1.585639e-02	6.562312e-01	8.409286e-01	8.403489e-01	2.121941e+00	2.090115e+00	1.274882e+00

Table 2

Group means and probabilities for LDA

Synthesis route	Yield	UTS	E	VEC	Atom_Size_Diff	dHmix	Probabilities
ST_6	134.83	227.50	82.64	2.06	0.02	-205.55	0.86667
ST_4	211.00	318.00	49.35	2.10	0.04	-1380.06	0.66667
DC	291.23	490.46	141.31	2.36	0.07	-4652.25	0.78889
IM	92.29	260.86	72.93	2.06	0.03	-265.06	0.75556
DMD	151.00	256.00	75.14	2.06	0.03	-472.24	0.82222

Table 3

LDA analysis of properties with respect to synthesis route and phases

With respect to synthesis route					
Properties	LD1	LD2	LD3	LD4	LD5
Yield	-0.0184	-0.0117	-0.0252	-0.0065	-0.0190
UTS	-0.0220	0.0030	0.0009	0.0312	0.0244

E	-0.0141	-0.0112	-0.0161	-0.0173	0.0204
VEC	-139.2761	-0.0336	109.955	-11.2031	53.0878
dHmix	0.3439	0.7202	-0.19009	-0.0224	-0.1408

With respect to phases

Property	LD1	LD2	LD3	LD4
Yield	-0.1449	-0.0371	-0.0782	-0.0121
UTS	0.0058	0.0674	0.0332	-0.0284
E	0.0263	-0.0582	0.0028	-0.0454
VEC	35.992	-92.789	31.0342	3.6329
Atom_Size_Diff	608.67	92.705	-69.6795	-148.965
dHmix	-0.0041	-0.0039	0.0007	-0.0039

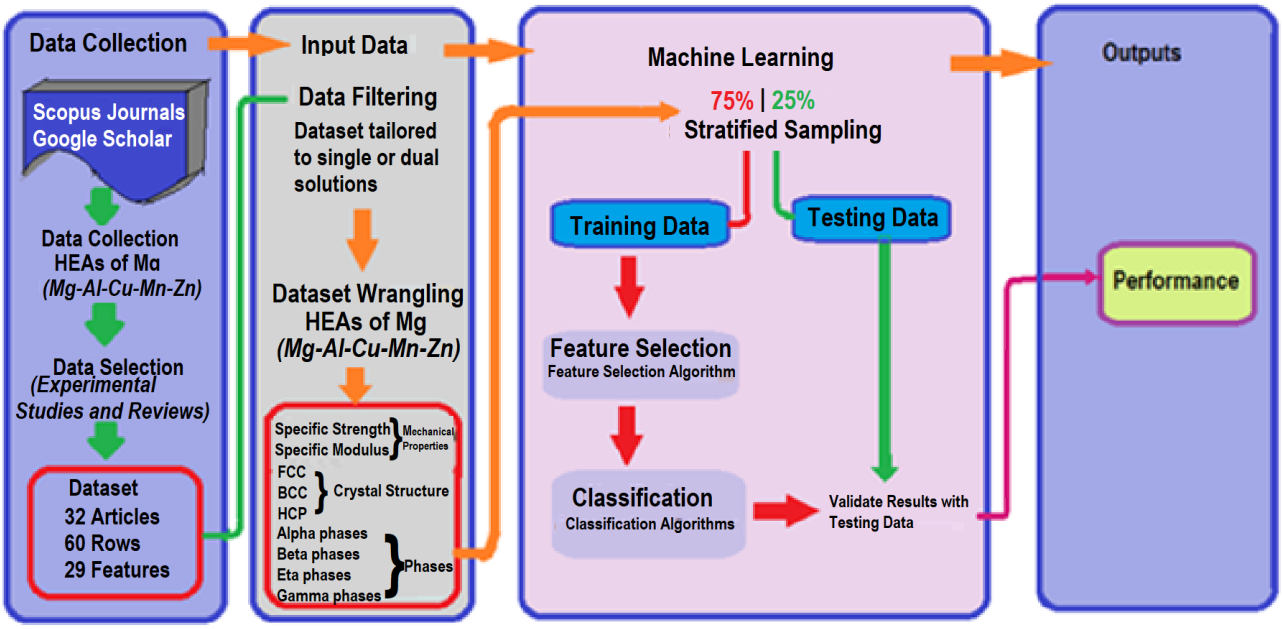

Figure 1. Phase and mechanical properties classification framework for ML

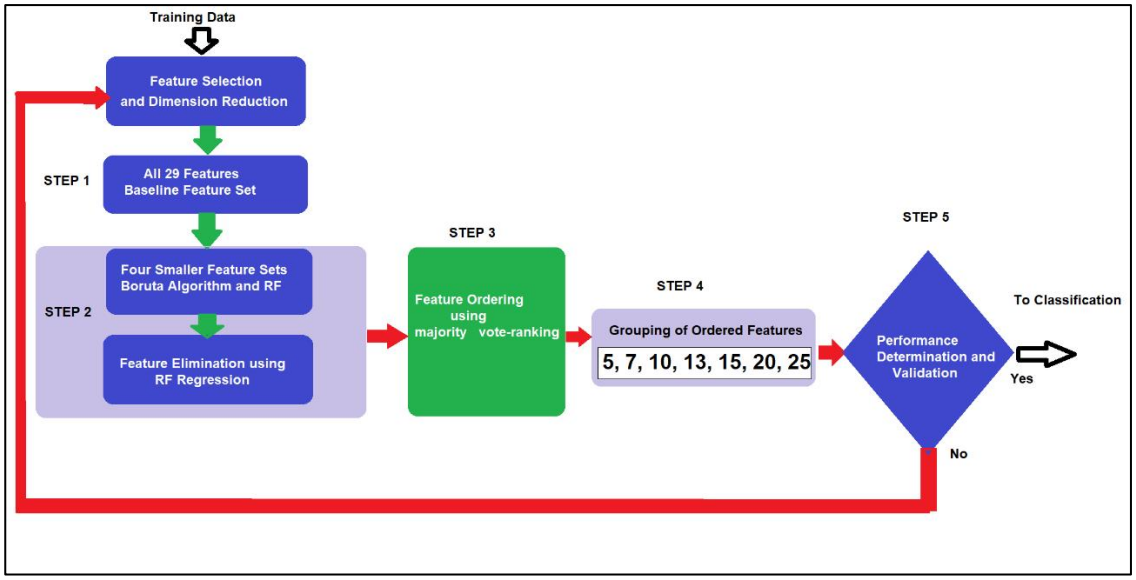

Figure 2 Feature selection

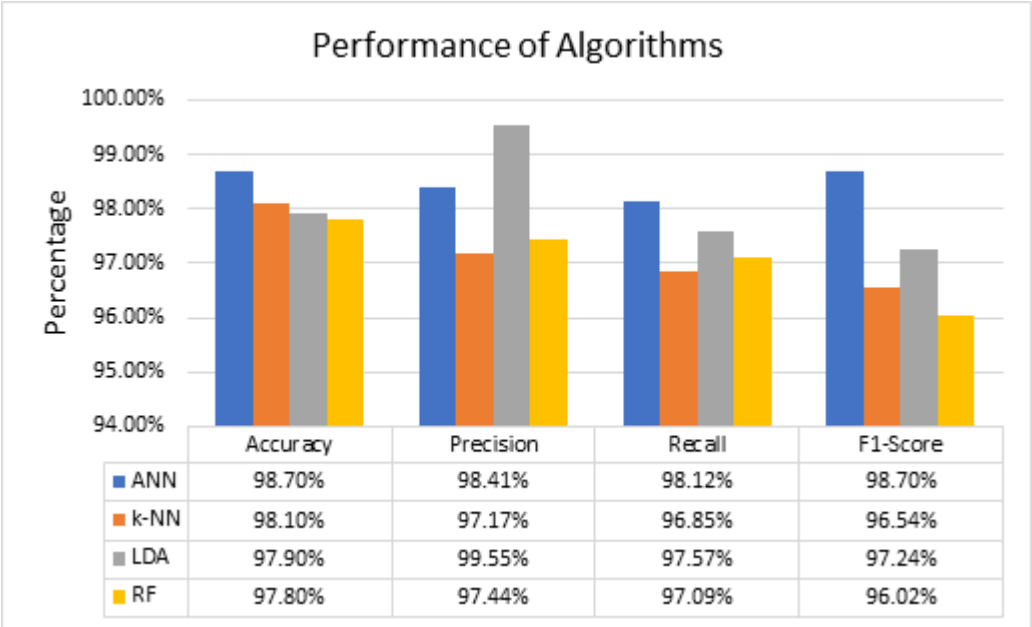

	Accuracy	Precision	Recall	F1-Score
ANN	98.70%	98.41%	98.12%	98.70%
k-NN	98.10%	97.17%	96.85%	96.54%
LDA	97.90%	99.55%	97.57%	97.24%
RF	97.80%	97.44%	97.09%	96.02%

Figure 3 Performance of the algorithms

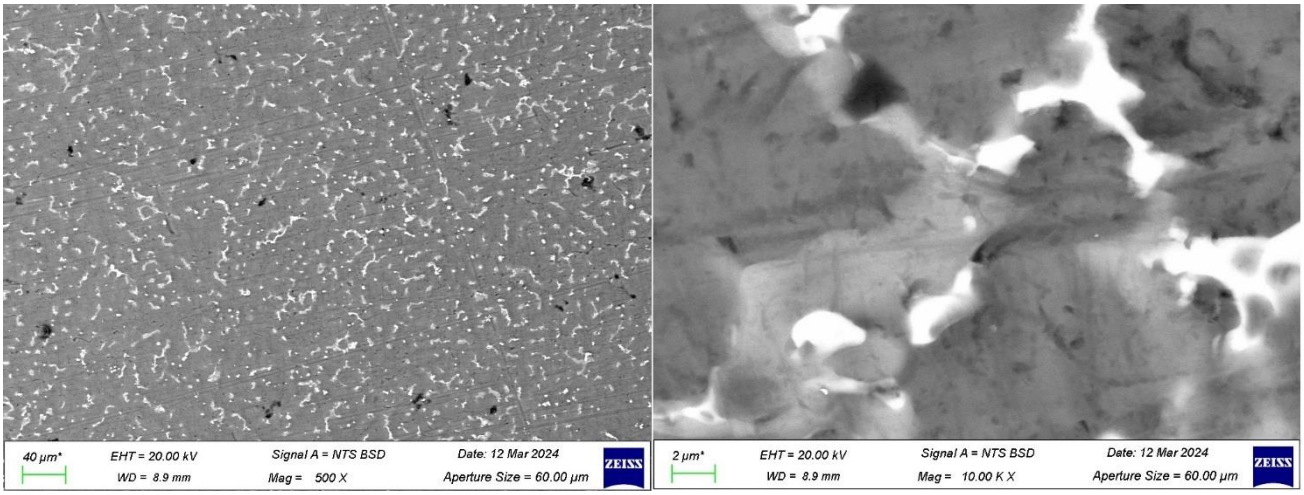

Figure 4 Tested alloy showing grain boundaries at X500 and X10,000

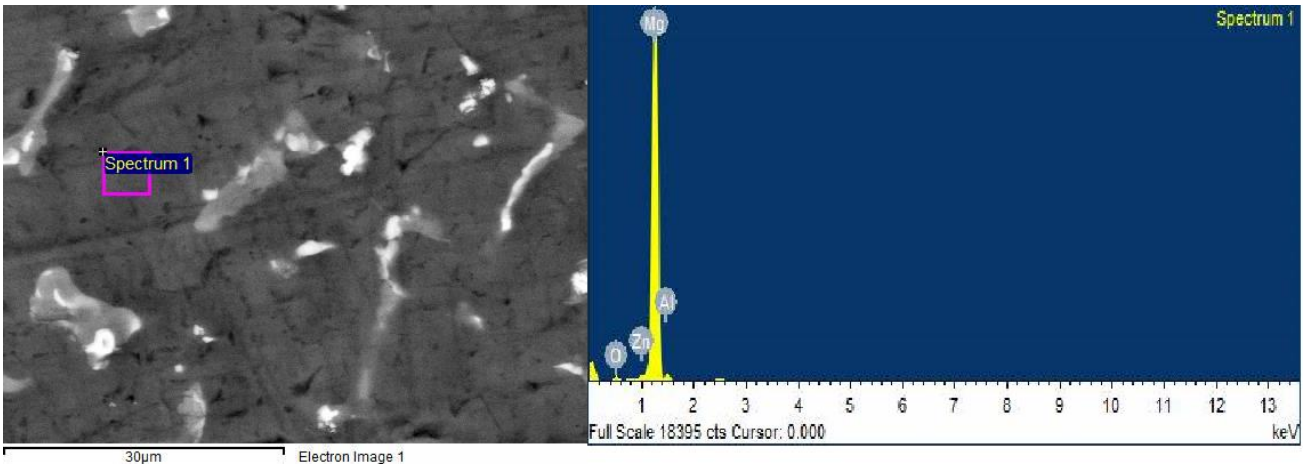

Figure 5 EDS Spectrum 1 and point of its collection

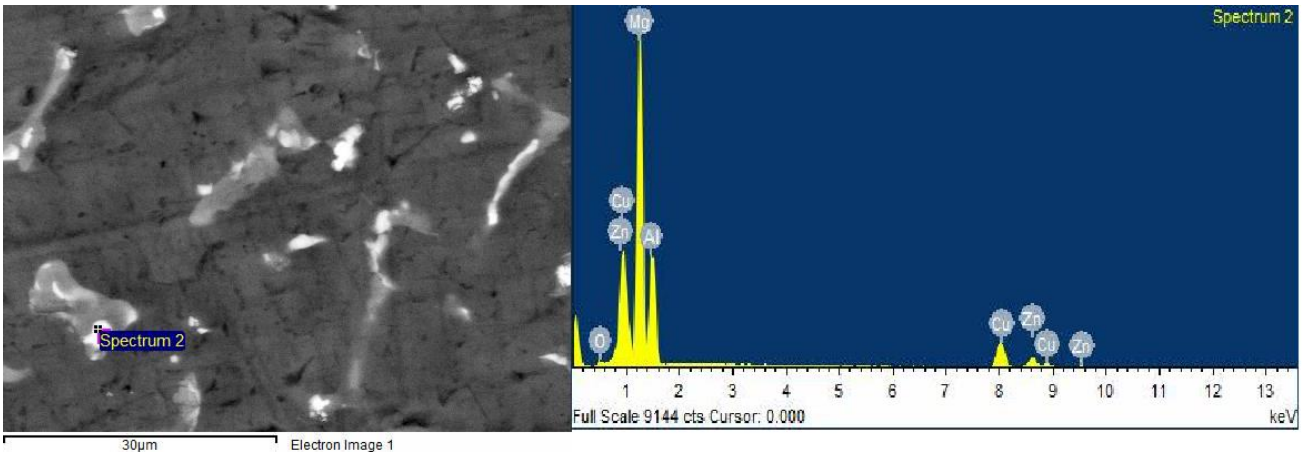

Figure 6 EDS spectrum 2 and point of its collection

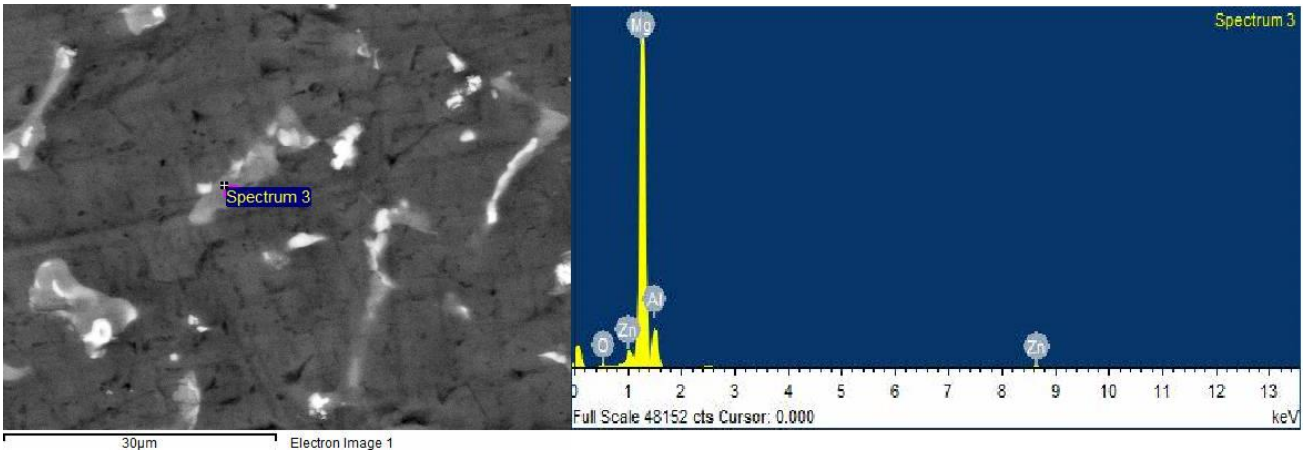

Figure 7 EDS Spectrum 3 and point of its collection

References

Behera, A., Sahoo, A.K., Mohapatra, S.S., 2022. Nickel–titanium smart hybrid materials for automotive industry, in: Thomas, S., Behera, Ajit, Nguyen, T.A. (Eds.), Nickel-Titanium Smart Hybrid Materials, Micro and Nano Technologies. Elsevier, pp. 271–295. https://doi.org/10.1016/B978-0-323-91173-3.00015-8

Bhandari, U., Zhang, C., Yang, S., 2020. Mechanical and Thermal Properties of Low-Density Al20+xCr20-xMo20-yTi20V20+y Alloys. Crystals 10, 278. https://doi.org/10.3390/cryst10040278

Bilbao, Y., Trujillo, J.J., Vicario, I., Arruebarrena, G., Hurtado, I., Guraya, T., 2022. X-ray Thermo-Diffraction Study of the Aluminum-Based Multicomponent Alloy Al58Zn28Si8Mg6. Materials 15, 5056. https://doi.org/10.3390/ma15145056

Chen, C., Liu, D., Deng, S., Zhong, L., Chan, S.H.Y., Li, S., Hng, H.H., 2021. Accurate machine learning models based on small dataset of energetic materials through spatial matrix featurization methods. J. Energy Chem., In Celebration of the 100th anniversary of Chemisry at Nankai University 63, 364–375. https://doi.org/10.1016/j.jechem.2021.08.031

Chen, X., Liao, Q., Niu, Y., Jia, W., Le, Q., Cheng, C., Yu, F., Cui, J., 2019a. A constitutive relation of AZ80 magnesium alloy during hot deformation based on Arrhenius and Johnson–Cook model. J. Mater. Res. Technol. 8, 1859–1869. https://doi.org/10.1016/j.jmrt.2019.01.003

Chen, X., Liao, Q., Niu, Y., Jia, Y., Le, Q., Ning, S., Hu, C., Hu, K., Yu, F., 2019b. Comparison study of hot deformation behavior and processing map of AZ80 magnesium alloy casted with and without ultrasonic vibration. J. Alloys Compd. 803, 585–596. https://doi.org/10.1016/j.jallcom.2019.06.242

Chen, X., Ning, S., Wang, A., Le, Q., Liao, Q., Jia, Y., Cheng, C., Li, X., Atrens, A., Yu, F., 2020. Microstructure, mechanical properties and corrosion behavior of quasicrystal-reinforced Mg-Zn-Y alloy subjected to dual-frequency ultrasonic field. Corros. Sci. 163, 108289. https://doi.org/10.1016/j.corsci.2019.108289

Dong, S., Wang, Y., Li, J., Li, Y., Wang, L., Zhang, J., 2024. Machine Learning Aided Prediction and Design for the Mechanical Properties of Magnesium Alloys. Met. Mater. Int. 30, 593–606. https://doi.org/10.1007/s12540-023-01531-6

Fan, Z., Baranovas, G., A. Yu, H., Szczęsny, R., Liu, W.-R., H. Gregory, D., 2021. Ultra-rapid synthesis of the MgCu 2 and Mg 2 Cu Laves phases and their facile conversion to nanostructured copper with controllable porosity; an energy-efficient, reversible process. Green Chem. 23, 6936–6944. https://doi.org/10.1039/D1GC01710A

Feng, R., Gao, M.C., Lee, C., Mathes, M., Zuo, T., Chen, S., Hawk, J.A., Zhang, Y., Liaw, P.K., 2016. Design of Light-Weight High-Entropy Alloys. Entropy 18, 333. https://doi.org/10.3390/e18090333

Ford, E., Maneparambil, K., Rajan, S., Neithalath, N., 2021. Machine learning-based accelerated property prediction of two-phase materials using microstructural descriptors and finite element analysis. Comput. Mater. Sci. 191, 110328. https://doi.org/10.1016/j.commatsci.2021.110328

He, X., Liu, J., Yang, C., Jiang, G., 2023. Predicting thermodynamic stability of magnesium alloys in machine learning. Comput. Mater. Sci. 223, 112111.

Li, J.-H., Tsai, M.-H., 2020. Theories for predicting simple solid solution high-entropy alloys: Classification, accuracy, and important factors impacting accuracy. Scr. Mater. 188, 80–87. https://doi.org/10.1016/j.scriptamat.2020.06.064

Li, Y., Guo, W., 2019. Machine-learning model for predicting phase formations of high-entropy alloys. Phys. Rev. Mater. 3, 095005. https://doi.org/10.1103/PhysRevMaterials.3.095005

Liu, Y., Wang, L., Zhang, H., Zhu, G., Wang, J., Zhang, Y., Zeng, X., 2021. Accelerated development of high-strength magnesium alloys by machine learning. Metall. Mater. Trans. A 52, 943–954.

Machaka, R., 2021. Machine learning-based prediction of phases in high-entropy alloys. Comput. Mater. Sci. 188, 110244. https://doi.org/10.1016/j.commatsci.2020.110244

Mandal, P., Choudhury, A., Basu, M.A., Ghosh, M., 2022. Phase Prediction in High Entropy Alloys by Various Machine Learning Modules Using Thermodynamic and Configurational Parameters. Met. Mater. Int.

Mi, X., Tian, L., Tang, A., Kang, J., Peng, P., She, J., Wang, H., Chen, X., Pan, F., 2022. A reverse design model for high-performance and low-cost magnesium alloys by machine learning. Comput. Mater. Sci. 201, 110881.

Pei, Z., Yin, J., Hawk, J.A., Alman, D.E., Gao, M.C., 2020. Machine-learning informed prediction of high-entropy solid solution formation: Beyond the Hume-Rothery rules. Npj Comput. Mater. 6, 1–8. https://doi.org/10.1038/s41524-020-0308-7

Qiao, L., Liu, Y., Zhu, J., 2021. A focused review on machine learning aided high-throughput methods in high entropy alloy. J. Alloys Compd. 877, 160295.

Reza Kashyzadeh, K., Amiri, N., Maleki, E., Unal, O., 2023. A Critical Review on Improving the Fatigue Life and Corrosion Properties of Magnesium Alloys via the Technique of Adding Different Elements. J. Mar. Sci. Eng. 11, 527.

Stergiou, K., Ntakolia, C., Varytis, P., Koumoulos, E., Karlsson, P., Moustakidis, S., 2023. Enhancing property prediction and process optimization in building materials through machine learning: A review. Comput. Mater. Sci. 220, 112031. https://doi.org/10.1016/j.commatsci.2023.112031

Tayyebi, M., Adhami, M., Karimi, A., Davood Rahmatabadi, Alizadeh, M., Hashemi, R., 2021. Effects of strain accumulation and annealing on interfacial microstructure and grain structure (Mg and Al3Mg2 layers) of Al/Cu/Mg multilayered composite fabricated by ARB process. J. Mater. Res. Technol. 14, 392–406. https://doi.org/10.1016/j.jmrt.2021.06.032

Tun, K.S., Kumar, A., Gupta, M., 2019. Introducing a High Performance Mg-Based Multicomponent Alloy as an Alternative to Al-Alloys. Front. Mater. 6.

Xiong, W., Cheng, L., Zhan, S., Guo, A.X., Liaw, P.K., Cao, S.C., 2023. Recent Advances on Lightweight High-Entropy Alloys: Process, Design, and Applications. High Entropy Alloys Mater. 1–20.

Xu, P., Ji, X., Li, M., Lu, W., 2023. Small data machine learning in materials science. Npj Comput. Mater. 9, 1–15. https://doi.org/10.1038/s41524-023-01000-z

Yamanoglu, R., Bahador, A., Kondoh, K., Gumus, S., Gokce, S., Muratal, O., 2021. New Magnesium Composite with Mg 17 Al 12 Intermetallic Particles. Powder Metall. Met. Ceram. 60, 216–224.